Particle & Particle Systems Characterization
www.particle-journal.com

In Vitro Evaluation of Non-Protein Adsorbing Breast Cancer Theranostics Based on ^{19}F-Polymer Containing Nanoparticles

Christian Porsch, Yuning Zhang, Åsa Östlund, Peter Damberg, Cosimo Ducani, Eva Malmström, and Andreas M. Nyström**

Eight fluorinated nanoparticles (NPs) are synthesized, loaded with doxorubicin (DOX), and evaluated as theranostic delivery platforms to breast cancer cells. The multifunctional NPs are formed by self-assembly of either linear or star-shaped amphiphilic block copolymers, with fluorinated segments incorporated in the hydrophilic corona of the carrier. The sizes of the NPs confirm that small circular NPs are formed. The release kinetics data of the particles reveals clear hydrophobic core dependence, with longer sustained release from particles with larger hydrophobic cores, suggesting that the DOX release from these carriers can be tailored. Viability assays and flow cytometry evaluation of the ratios of apoptosis/necrosis indicate that the materials are non-toxic to breast cancer cells before DOX loading; however, they are very efficient, similar to free DOX, at killing cancer cells after drug encapsulation. Both flow cytometry and confocal microscopy confirm the cellular uptake of NPs and DOX-NPs into breast cancer cells, and in vitro ^{19}F-MRI measurement shows that the fluorinated NPs have strong imaging signals, qualifying them as a potential in vivo contrast agent for ^{19}F-MRI.

1. Introduction

Today, cancer is one of the leading causes of death in the industrialized world, becoming more prevalent with our longer life spans, making this an increasingly important research area. As the most common type of cancer among women, breast cancer has attracted significant attention from scientists worldwide. Traditional treatments for breast cancer, such as chemotherapy, radiation, and surgery, have been effective in treating women over the last decades, but are associated with both discomfort and sometimes severe side effects for patients.

Doxorubicin (DOX), one of the most commonly used chemotherapeutics in the clinic, is employed to treat many different types of cancer, including bladder, lung, ovarian and breast cancer.[1–4] However, similar to many other anti-cancer drugs, DOX has severe issues with toxicity, and can cause cardiac damage.[5] Consequently, in the past few decades, several different nanoscale systems have been investigated as new delivery platforms for DOX in order to increase efficacy and reduce side effects such as bystander tissue damage as well as to modify the pharmacokinetics of the pharmaceutical. Further, with nanoscale formulation multi drug resistance (MDR) could be overcome, via control of the pharmacokinetics and biodistribution of the drug and alternative tumor uptake mechanisms.[6–13] By such sophisticated nanomedical approaches to chemotherapy, advantageous synergistic effects in terms of enhanced drug solubility, tissue protection, drug circulation time, and selective drug accumulation can be accomplished.[8,14] For this purpose, polymer platforms have attracted substantial focus due to their engineered biocompatibility, biodegradability, and extensive versatility.[15–17] More recently, significant focus has been directed towards the design of dual-functional delivery platforms, which provide both a therapeutic and a diagnostic function, so called theranostics.[18,19] The advantages of such systems are complementary to the chemotherapeutic effect, in that theranostic systems can give simultaneous information regarding tumor heterogeneity, metastasis, and therapeutic efficacy.[20,21] One popular approach to develop such theranostic entities is to combine the

C. Porsch, Prof. E. Malmström
KTH Royal Institute of Technology
School of Chemical Science and Engineering
Department of Fibre and Polymer Technology
100 44, Stockholm, Sweden
E-mail: mavem@kth.se
Y. Zhang, Dr. C. Ducani, Prof. A. M. Nyström
Swedish Medical Nanoscience Center
Department of Neuroscience
Karolinska Institutet
171 77, Stockholm, Sweden
E-mail: andreas.nystrom@ki.se
Dr. Å. Östlund
Applied Surface Chemistry
Department of Chemical and Biological Engineering
Chalmers University of Technology
412 96, Gothenburg, Sweden
Prof. P. Damberg
Division of Medical Imaging and Technology
Department of Clinical Science
Intervention and Technology (CLINTEC)
Karolinska Institutet
171 77, Stockholm, Sweden

DOI: 10.1002/ppsc.201300018

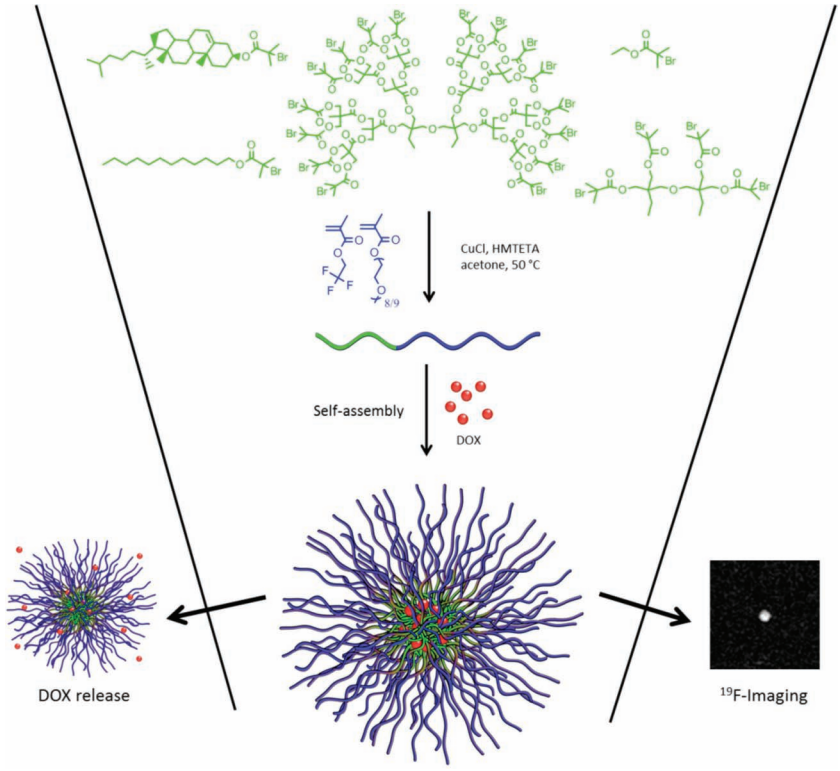

Figure 1. Synthetic strategy to the theranostic NPs, where hydrophobic segments are visualized in green and hydrophilic segments in blue.

therapeutic delivery with an imaging modality, such as radionuclides for positron emission tomography (PET), computed tomography (CT), or magnetic resonance imaging (MRI).[21] While PET and CT rely on radioactive nuclides and ionization radiation, respectively, MRI is a non-invasive imaging technique that provides good visualization of soft tissue with good spatial resolution. Further, its non-radioactive nature makes MRI suitable for use in treatment regiments that require multiple injections. Typically, chelates of paramagnetic compounds such as gadolinium (Gd^{3+})[22,23] and superparamagnetic iron-oxide nanoparticles (SPIONs),[24–26] have been proposed as contrast agents for theranostic delivery. However, accumulation and toxicity of the Gd^{3+} ion, due to release from its chelated form, and potential toxicity of SPIONs[27] may be an issue for theranostic purposes. Recently, the use of the natural isotope ^{19}F has emerged as a promising alternative to these conventional paramagnetic agents for imaging.[28–35] Good biocompatibility and low background signal in vivo are attractive properties of the fluorine atom, although relatively low sensitivity requires comparatively high concentrations for MRI applications. However, previous work has highlighted the importance of providing nanoparticle (NP) platforms that allow for high fluorine content and mobility of the ^{19}F-atoms in order to provide beneficial relaxation properties.[28] Further, very few reports have used fluorinated polymers to construct theranostic NPs using chemotherapeutics such as DOX.[29] Therefore, we herein present a versatile route to synthesize fluorinated polymer NPs, which are detectable by ^{19}F-MRI, and able to encapsulate and deliver DOX, to combat breast cancer as a theranostic system. The characteristics of the NPs were established with conventional analytical techniques, and ^{19}F-NMR diffusion was used as a novel method to define their size in complex media such as plasma. Furthermore, the theranostic properties were evaluated by ^{19}F-MRI measurements and an array of cell-based assessments.

2. Results and Discussion

2.1. Synthesis and Characterization of Fluoro-Containing Amphiphilic Polymers

In the present work, a facile method to produce fluoro-containing polymer nanoparticles (NPs) is presented, as schematically shown in **Figure 1**. Amphiphilic polymers with different hydrophobic segments and similar hydrophilic segments were spontaneously self-assembled to yield stable core-shell type NPs. By random introduction of fluorine atoms along the hydrophilic segment of the polymer, NPs with very high fluorine content have been realized, which thereby, facilitate high sensitivity ^{19}F-MRI phantom imaging. Simultaneously, the hydrophobic NP core allows for loading and protection of therapeutic cargos, thus rendering a versatile dual-functional theranostic delivery platform.

A library of amphiphilic polymers of different architectures was synthesized in a two-step strategy. In the first part, a number of different linear low molecular weight or low generation dendritic hydrophobic core molecules were designed and equipped with atom transfer radical polymerization (ATRP) initiating groups. The syntheses were conducted by employing standard base catalyzed esterification reactions, described in the Supporting Information, and the structural integrity of the products was confirmed by ^{1}H-NMR (Supporting Information Figure S1). In the second part of the synthesis, the initiating moieties were utilized to polymerize hydrophilic statistical copolymers of the monomers oligo(ethylene glycol) methyl ether methacrylate (OEGMA (average M_n = 475)) and trifluoroethyl methacrylate (TFEMA) via ATRP. In this manner, either linear or star-shaped (4 or 16 arms) amphiphilic polymers were produced and subsequently characterized by ^{1}H-NMR and SEC analysis (**Table 1** and Supporting Information Figure S2–S4). The first part of the names in Table 1 denotes the hydrophobic segment of the polymer and the subscript number represents the total molecular weight of the amphiphilic polymer. TFEMA was chosen as the contrast agent due to its commercial availability as well as its chemically equivalent fluorine atoms, which is optimal for NMR imaging since it results in no dilution of the NMR signal. OEGMA has emerged as a promising alternative to PEGylation,[36,37] and its hydrophilic and highly dynamic structure is hypothesized to facilitate the mobility of the fluorine atoms of TFEMA.

Table 1. Summary of the characteristics of the prepared polymers.

Polymer[a)]	Abbreviation	Type	OEGMA:TFEMAb)	F-content[b)] [wt%]	M_n[c)] [g mol^{-1}]	M_n/arm[c)] [g mol–1]	Đ[c)]
EBiB-P(OEGMA-*co*-TFEMA)	EBiB-P(O-*co*-T)	Linear	51:49	8.9	25 300	–	1.17
Dodecanol-P(OEGMA-*co*-TFEMA)	Dod-P(O-*co*-T)	Linear	48:52	9.5	21 500	–	1.14
Cholesterol-P(OEGMA-*co*-TFEMA)	Chol-P(O-*co*-T)	Linear	44:56	10.6	21 300	–	1.16
diTMP-[G#0]-P(OEGMA-*co*-TFEMA)$_{10k}$	[G#0]-P(O-*co*-T)$_{10k}$	Star (4 arms)	49:51	8.8	10 300	2400	1.22
diTMP-[G#0]-P(OEGMA-*co*-TFEMA)$_{28k}$	[G#0]-P(O-*co*-T)$_{28k}$	Star (4 arms)	50:50	8.6	27 900	6900	1.13
diTMP-[G#2]-P(OEGMA-*co*-TFEMA)$_{23k}$	[G#2]-P(O-*co*-T)$_{23k}$	Star (16 arms)	44:56	4.4	22 500	1200	1.10
diTMP-[G#2]-P(OEGMA-*co*-TFEMA)$_{36k}$	[G#2]-P(O-*co*-T)$_{36k}$	Star (16 arms)	47:53	5.4	36 000	2100	1.05
diTMP-[G#2]-P(OEGMA-*co*-TFEMA)$_{52k}$	[G#2]-P(O-*co*-T)$_{52k}$	Star (16 arms)	49:51	6.2	52 000	3100	1.10

[a)]The first part of the name denotes the hydrophobic segment of the polymer, and the subscript number represents the total molecular weight of the amphiphilic polymer; [b)]H-NMR; [c)]DMF-SEC. Ref. [38].

Following this procedure, three linear polymers with different hydrophobic core moieties were synthesized, with a comparable molecular weight of the hydrophilic segment, to determine the effect of the core on the NP characteristics and the drug release behavior. Additionally, five star polymers were synthesized from either a [G#0] (4 arms) or [G#2] (16 arms) dendrimer core. In addition to the differences in the hydrophobic core size and number of hydrophilic arms of the [G#0] and [G#2] cores, the molecular weight of the hydrophilic segment was also varied to evaluate the possible impact of M_n on the material performance (Table 1). All polymerizations were conducted in acetone using a HMTETA/CuCl mediated system and proceeded in a controlled manner with reproducible kinetics (Supporting Information Figure S5). The reactions were monitored by ^{1}H-NMR and allowed to run to 30–50% conversion to obtain control over the final products. All polymers typically show dispersities ($Đ$[38] of 1.1–1.2 as determined by SEC (Table 1 and Supporting Information Figure S6). Remaining trace amounts of copper in the polymers were removed by dialysis against an aqueous EDTA solution. By incorporation of fluorinated monomers into the hydrophilic segments of the polymers, very high fluorine content was accomplished, and similar monomer compositions of the hydrophilic segments (49–56 mol% of TFEMA) were achieved for all materials. Despite the high fluorine content, all materials are soluble in both water and phosphate buffered saline (PBS) up to concentrations of 15 mg mL^{-1}. High fluorine content is of utmost importance to obtain a high signal in MRI since fluorine atoms only have about 83% sensitivity compared to protons.[39,40] Additionally, during polymerization, it was discovered that the reactivity of TFEMA is higher than of OEGMA. Consequently, the resulting polymers are expected to have a tapered composition with statistically more TFEMA closer to the core, and increasing amounts of OEGMA towards the chain ends.[41]

2.2. Nanoparticle Formation

Micellization of the polymers was conducted by first dissolving them in dichloromethane (DCM), a good solvent for the hydrophobic core. Subsequently, PBS was slowly added to the solution and the DCM was evaporated during gentle stirring (100 rpm) for 36 h to form the core-shell particles. The synthesized polymers readily formed micelles as observed by dynamic light scattering (DLS) and transmission electron microscopy (TEM) (**Table 2** and Supporting Information Figure S1; **Figure 2** and Supporting Information Figure S7). DLS results show that all polymers self-assemble into relatively small NPs with diameters

Table 2. Summary of NP sizes with and without DOX-loading, determined by DLS and TEM. CMCs for the synthesized polymers in PBS solution.

	NPs		DOX-NPs		
	$D_{h,v}$[a)] [nm]	D_h[b)] [nm]	$D_{h,v}$[a)] [nm]	D_h[b)] [nm]	CMC[c)] [μg mL^{-1}]
EBiB-P(O-*co*-T)	5.9 ± 0.2	14 ± 4	920 ± 50	10 ± 2	3.0
Dod-P(O-*co*-T)	6.3 ± 0.1	15 ± 3	1180 ± 200	11 ± 2	3.8
Chol-P(O-*co*-T)	6.9 ± 0.2	10 ± 3	860 ± 70	20 ± 3	2.2
[G#0]-P(O-*co*-T)$_{10k}$	7.3 ± 0.6	9 ± 2	1100 ± 170	10 ± 2	1.8
[G#0]-P(O-*co*-T)$_{28k}$	6.8 ± 0.4	10 ± 2	1030 ± 60	13 ± 4	1.8
[G#2]-P(O-*co*-T)$_{23k}$	7.0 ± 0.1	10 ± 2	1030 ± 160	8 ± 2	1.1
[G#2]-P(O-*co*-T)$_{36k}$	7.1 ± 0.3	7 ± 1	900 ± 110	16 ± 5	0.82
[G#2]-P(O-*co*-T)$_{52k}$	9.0 ± 0.2	8 ± 2	1420 ± 140	9 ± 2	1.3

[a)]DLS (25 °C); [b)] TEM; [c)]Fluorescent probe technique.

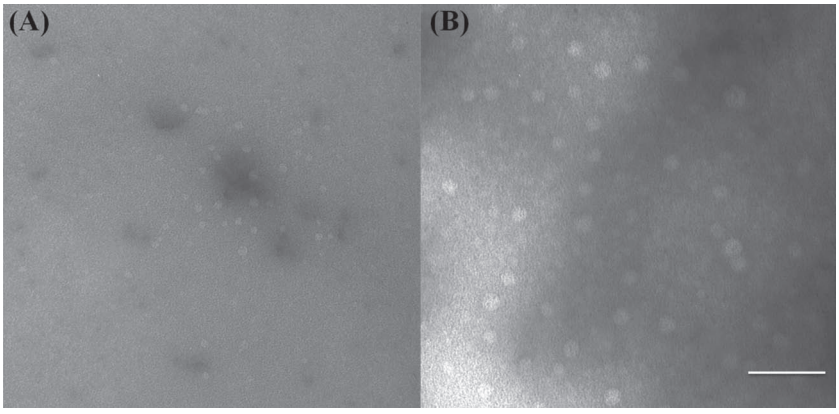

Figure 2. TEM images of NPs and DOX-NPs A) Chol-P(O-*co*-T) and B) DOX-Chol-P(O-*co*-T). Scale bar = 100 nm in both images.

in the range of 6-9 nm in PBS. TEM confirms that the particles formed are circularly shaped with a relatively narrow size distribution, and NP sizes from TEM (7–15 nm) are generally larger than those observed by DLS (Table 2). The small NP sizes are in proximity to the reported threshold for renal clearance.[42] Furthermore, recent studies report the topologic nature of the polymer as an influencing factor.[43,44] It is possible that star-shaped polymers may be beneficial in this context since they have a more restricted reptation and therefore longer circulation times.[43] The increase in size with increasing length of the hydrophilic segment of the [G#2]-core polymers is expected due to increased extension of the NP shell. However, the size decrease of the [G#0]-core polymers are more surprising. This may be an effect of the relatively large change in hydrophilic/hydrophobic ratio of the [G#0] polymers, thus resulting in different aggregation numbers of the self-assembled structures.

To confirm the applicability of the synthesized NPs for physiological delivery, the stability of the NPs upon dilution is of significant importance to avoid particle disassembly upon injection into the blood stream. Such instant disassembly may result in a burst release of the therapeutic cargo without any controlled release function. The critical micelle concentrations (CMCs) of the NPs were determined by employing the pyrene probe technique using fluorescence spectroscopy (Table 2 and Supporting Information Figure S8).[45] All polymers show very low CMCs (0.8-3.8 μg mL^{-1}), thus confirming their NP stability upon dilution. Further, the lower CMC values for the star-shaped polymers suggests that they are more prone to form NPs, possibly with a lower aggregation number than the linear polymers. However, the star polymers still show an assembly behavior, which indicates that they do no not form discrete unimolecular NPs.

2.3. ^{19}F-NMR and ^{19}F-NMR Diffusion Studies of NPs in Complex Media

Three of the synthesized NPs; EBiB-P(O-*co*-T), Chol-P(O-*co*-T), and [G#0]-P(O-*co*-T)$_{28k}$, were chosen as model compounds to be evaluated with respect to their relaxation behavior (a representative ^{19}F-NMR is reported in Supporting Information Figure S9). The relaxation parameters (T_1 and T_2) of the NPs were measured employing a 600 MHz NMR instrument, and are reported in Table S4 (Supporting Information). As expected, all T_1 and T_2 relaxations are very similar, thus indicating that the chemical surroundings of the fluorine atoms in the different NPs, regardless of the architecture of the hydrophobic core, are fairly equal. Furthermore, the beneficially short T_1 relaxation time (compared to low M_w compounds) of approximately 320 ms for all materials is most likely a consequence of linking the fluorine-containing monomers to a high molecular weight polymer. T_2 relaxation times are somewhat lower than expected (5–8 ms), thus indicating that the mobility of the fluorine atoms in the dynamic OEGMA segments is not as high as anticipated.

The fact that fluorine is covalently incorporated in the NP structure results in a unique possibility to characterize NP sizes in plasma-containing media, and investigate the effect of proteins on the size of the NPs. Although, it is widely accepted that PEGylation of NPs results in prolonged circulation time in vivo, there are, to the authors' best knowledge, few studies that report the determination of NP sizes in plasma.[46] Therefore, we hereby report ^{19}F-NMR diffusion as a novel and attractive approach to determine the size of fluorinated NPs in complex media. Due to the unique fluorine signal from our NPs, ^{19}F-NMR diffusion can be employed to determine the size of the NPs in protein rich media as Dulbecco's modified Eagle medium (DMEM) with fetal bovine serum (FBS), and even in plasma without any measurement interferences. Table S4 (Supporting Information) presents the NP sizes of the three model polymers in PBS, DMEM, and plasma measured by ^{19}F-NMR diffusion. All NPs have somewhat smaller sizes when determined by ^{19}F-NMR diffusion compared to DLS, which is expected since NMR diffusion is known to overestimate smaller objects rather than larger objects as is the case with DLS. Furthermore, the NP sizes from ^{19}F-NMR in different media indicate that increasing the complexity of the surroundings decreases the diameter of the NPs. This could be an effect of reduced solubility of the polymers (due to changes in ionic strength, salt types and concentrations or protein content), thus causing the NPs to shrink, suggesting that this phenomena should be further investigated in the future. However, this fact also clearly suggests that the NP corona is not subjected to any measureable protein adsorption that would have been seen in a size increase in our experimental timeframe. Conclusively, we can, via this technique, confirm that the P(OEGMA-*co*-TFEMA) exterior provides a stealthy corona to the NPs. This is mainly believed to be an effect of the stealth properties known for PEGylated polymers, however, the good antifouling properties of fluorine against proteins may also contribute to this effect.

2.4. DOX Loading and In Vitro Release

The loading efficiency of DOX into the different polymers is at similar level, from 70–89% (Supporting Information Table S5).

Generally, [G#2]-polymers show a higher loading efficiency than [G#0]-polymers and the loading efficiency decreases within the same generation when the molecular weight increases. This indicates that larger hydrophobic cores increase the loading capacity while larger hydrophilic shells decrease it. The Chol-P(O-*co*-T) material, similar to [G#2]-P(O-*co*-T)$_{23k}$, demonstrated the highest capability to encapsulate DOX (ca. 88%).

The sizes and shapes of the DOX loaded NPs were analyzed by DLS (25 °C) and TEM. Results from TEM show DOX-NPs with sizes in the range 8.3–19.5 nm (Table 2; Figure 2 and Supporting Information Figure S7), which is similar to the unloaded NPs. For DLS the three mean size parameters; intensity, number, and volume showed similar diameters for the different NPs (Table 2 and Supporting Information Figure S1). However, the size span of the different materials determined by DLS is far wider (800–1400 nm) than the diameters seen by TEM, and for the NPs prior to drug loading. This indicates that aggregation occurs after drug loading. To resolve this issue, several other loading methods were evaluated; with different organic solvents used for DOX (DMF, $CHCl_3$, THF, and acetone), altered stirring rates, using drop-wise addition of organic solvent or aqueous buffer, or dialysis under sink conditions to remove free DOX. These methods also resulted in similar or even greater degrees of aggregation. Consequently, it is likely that the DOX itself, rather than the loading method, contributes to the aggregation, and we are currently exploring other anthracyline derivatives as target drugs for encapsulation. Additionally, one possible explanation for the particle-particle interactions can be the presence of the fluorinated segments in the otherwise hydrophilic PEG-based corona of the NPs, resulting in DOX localizing partly in the corona upon loading. Hydrophobic interactions between DOX and the fluorinated segments, in combination with strong π–π interactions between DOX molecules, most likely explains the aggregation phenomena (especially at higher particle concentrations) seen from DLS to a large extent.

To reduce the interparticle aggregation phenomena seen for the DOX-loaded NPs, an additional material was synthesized with the hypothesis that aggregation can be suppressed by introduction of proper amounts of negatively charged components into the synthesized platforms. In this polymer, Chol-P(OEGMA-*co*-MMAc-*co*-TFEMA), around 50% of the OEGMA monomers were replaced by methacrylic acid (MAAc) monomers to form partly charged NPs (full experimental details and polymer characteristics (Table S3) are reported in the Supporting Information). The NP sizes obtained from DLS and TEM after DOX loading of the partly charged material (Table S2 and Figure S7) show that the interparticle aggregation seen for the other DOX-loaded NPs is significantly suppressed. This indicates that introduction of negative charge into the hydrophilic segments of the NPs results in chain repulsion and prevents aggregation after DOX loading. This improved NP behavior, as well as the possibilities for ligand mediated targeting approaches conjugated via these groups, will be further explored while developing the designed theranostic system for in vivo targeting.

The in vitro DOX release results for the different NPs are shown in **Figure 3**. All NPs show diffusion-controlled release profiles compared to free DOX (that diffuses out to more than 95% in 12 h). The release kinetics of the NPs show clear core

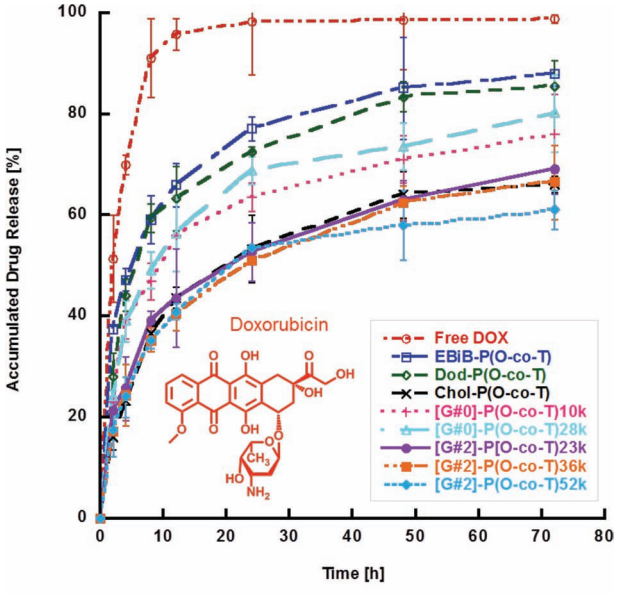

Figure 3. In vitro drug release of the DOX-loaded NPs. Samples were suspended in 4 L of PBS at 37 °C with magnetic stirring and protected from light.

dependence, thus suggesting the DOX release can be tailored by the polymer design. EBiB-P(O-*co*-T) and Dod-P(O-*co*-T) NPs have small hydrophobic cores, and consequently exhibit the highest DOX release rates (ca. 65% DOX within 12 h and 85% after 72 h), probably due to less pronounced hydrophobic interactions.

The dendritic core NPs show clear generation dependence from their release kinetics. The [G#0] cored NPs show a relatively fast release (56% in 12 h and 76–80% in 72 h), while [G#2]-cored NPs have a more sustained release (about 40% in 12 h and 61–69% in 72 h), which most likely is an effect of the substantially higher hydrophobicity of the [G#2] dendrimer core. Interestingly, the Chol-P(O-*co*-T) NPs shows a similar release profile compared to the [G#2] core materials. This is believed to be a consequence of π–π interactions between the ring structures of cholesterol and DOX, thus slowing down the drug diffusion, which has been previously observed for PS core NPs.[47] Conclusively, NPs with a larger hydrophobic core are better at keeping the drug entrapped in vitro, and cholesterol may be an interesting core moiety to provide controlled, sustained DOX release.

2.5. Cytotoxicity Tests

Four different cell lines (three breast cancer and one monocyte cell line) showed no obvious viability depression after incubation with the eight different polymers after 48 and 72 h, as evaluated with MTT tests (**Figure 4**A and Supporting Information Figure S10). Pure NPs were incubated at different concentrations from 0.01 to 500 μg mL^{-1} before DOX loading. At the highest concentration tested, 500 μg mL^{-1}, some materials reduced the cellular viability to around 90%, however; this

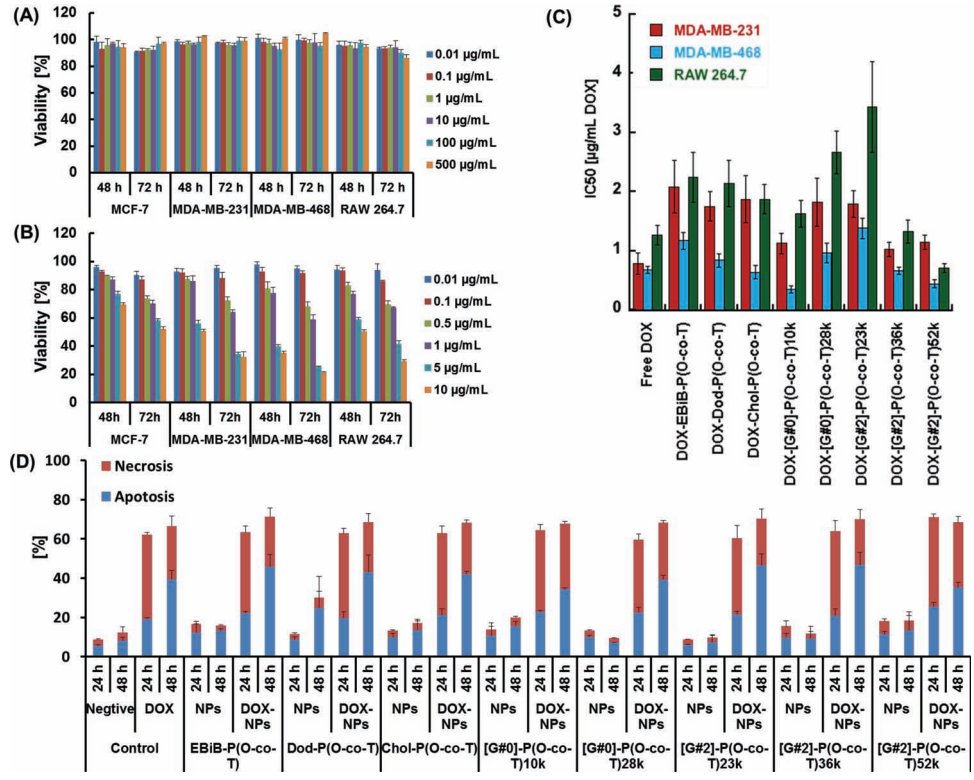

Figure 4. The effect of NPs and DOX-NPs on cell viability. A) Chol-P(*O-co*-T) and B) DOX-Chol-P(*O-co*-T), incubated with MCF-7, MDA-MB-231, MDA-MB-468, and RAW 264.7 cell lines for 48 h and 72 h. C) IC_{50} of MDA-MB-231, MDA-MB-468 and RAW 264.7 cells after treatment with free DOX or DOX-NPs for 72 h. D) Apoptosis/necrosis of NPs and DOX-NPs for the MDA-MB-231 cell line.

concentration is far above the possible in vivo concentration of NPs. Therefore, all NPs are considered to be non-toxic against the tested cancer cell lines.

The influences of free DOX and DOX-loaded NPs to the four cell lines were also evaluated by MTT assays (Figure 4B and Supporting Information Figure S11). Considering the DOX concentration of each sample, the same dose in the evaluation (10 µg mL^{-1}) was selected as the highest concentration for the assays. The viability of the four different cell lines was suppressed by DOX-NPs at different concentrations for both 48 and 72 h. Generally, the viability of the cells after incubation with DOX-containing NPs for 72 h was lower than for 48 h. In addition, different cell lines showed different level of sensitivity to DOX. MCF-7 was the least sensitive cell line, and even at the highest concentration in the test (10 µg mL^{-1} equivalents of DOX) the viability of the cells incubated with either DOX or DOX-NPs was still above 50%. Consequently, no accurate values of IC_{50} of the different DOX-NPs could be obtained for MCF-7 cells (Supporting Information Figure S11). For the other cell lines, MDA-MB-231, MDA-MB-468, and RAW 267.4, IC_{50} of DOX in the different carriers at 72 h, was calculated and is summarized in Figure 4C. It was found that the IC_{50} of free DOX in MDA-MB-231 and MDA-MB-468 cells were 0.77 µg mL^{-1} (1.33 µM) and 0.68 µg mL^{-1} (1.17 µM), respectively, which are in the same range as previous published studies (MDA-MB-231, 0.5 to 5 µM;[48–50] MDA-MB-468, 1.2 to 8 µM[51,52]. All materials show good carrier properties since they do not increase IC_{50} values significantly compared to free DOX for all three cell lines. MDA-MB-468 is the most sensitive cell line to DOX and DOX-NPs, and resulted in IC_{50} values below 1.5 µg mL^{-1} for all polymers. Further, DOX-Chol-P(O-*co*-T), DOX-[G#0]-P(O-*co*-T)$_{10k}$ and DOX-[G#2]-P(O-*co*-T)$_{52k}$ were found to have lower IC_{50} than free DOX. MDA-MB-231 is less sensitive to DOX-NPs than MDA-MB-468 cells, and all materials were found to have higher IC_{50} compared to free DOX. This increase in IC_{50} after DOX loading into the NPs has also been seen in other publications.[50,53]

The non-toxicity of NPs and toxicity effects of DOX-NPs against breast cancer cell lines were further evaluated by apoptosis/necrosis staining and quantitative evaluations of the cells via flow activated cell sorting (FACS). None of the NPs showed an obvious increase of cellular apoptosis or necrosis at 24 or 48 h of incubation with the three cell lines (Figure 4D and Supporting Information Figure S10). This indicates that the NPs themselves do not trigger programmed cell death. This in combination with the MTT assay results strongly suggests that the neat NPs can be considered as non-toxic to the cancer cells. However, DOX-NPs were found to be highly effective against breast cancer cells by increasing the total percentage of dead cells significantly. Generally, all cell lines displayed increased cell death after longer DOX-NPs incubation times for all materials. Interestingly, both MDA-MB-231 and MDA-MB-468 showed increased apoptosis and decreased necrosis levels after 48 h treatment with DOX-NPs compared to 24 h, indicating that

the apoptosis process is either slowed down or that the DOX-NPs can alter the pathway of cell death by triggering apoptosis.

According to the recent review by Fadeel et al. there are two major apoptosis pathways: the extrinsic or death receptor-mediated pathway, and the intrinsic or mitochondria-dependent pathway.[54] DOX can penetrate the nuclei membrane and intercalate with DNA,[55] and such cellular stress may trigger apoptosis via the intrinsic pathway.[56–58] However, we have not investigated the mechanism of apoptosis in detail in this manuscript, as the process and the signaling pathways leading to apoptosis are out of our scope and requires a dedicated effort by experts.[59,60] Further, the longer incubation times were found to result in higher death rates (Figure 4D and Supporting Information Figure S12), which is consistent with the MTT results that show a reduced viability of cancer cells after incubation with DOX-NPs for 72 h (Supporting Information Figure S11) compared to 48 h (data not shown). A lower apoptosis level was found by DOX-NPs in MCF-7 compared to the other two breast cancer cell lines. This suggests that MCF-7 cells might be able to resist DOX to some extent, which is consistent with the MTT results.

2.6. Cellular Uptake and Localization of NPs and DOX-NPs

Cellular uptake and localization of DOX and DOX-NPs was evaluated by FACS and confocal microscopy, respectively. The position movements of MDA-MB-468 cells, indicating DOX uptake after 24 and 48 h, are shown in Supporting Information Figure S13. For this cell line, the uptake of free DOX was found to be significantly ($p < 0.05$) higher than DOX-NPs after 48 h, while for the other cell lines no obvious difference was observed (Supporting Information Figure S14A). Furthermore, the cellular uptake of fluorescently labeled NPs, FITC-Chol-P(O-*co*-T) and FITC-[G#0]-P(O-*co*-T)$_{28k}$, was analyzed and compared to the negative control. The results in Supporting Information Figure S13E,K and F,L of cells treated with FITC-Chol-P(O-*co*-T) and FITC-[G#0]-P(O-*co*-T)$_{28k}$ confirms the NP uptake. For MCF-7 cells both time and NP dependent uptake increase was observed ($p < 0.001$), while for the MDA-MB-468 cells the uptake of FITC-[G#0]-P(O-*co*-T)$_{28k}$ was significantly higher compared to FITC-Chol-P(O-*co*-T) ($p < 0.001$) (Supporting Information Figure S14B).

To further evaluate the drug delivery efficacy of the NPs, the distribution of DOX and NPs were studied in cells. DOX-[G#0]-P(O-*co*-T)$_{28k}$ and DOX-Chol-P(O-*co*-T) NPs were incubated in cells for different time periods, and the same dose of free DOX was used as positive control. DOX-NPs favorably distributed similarly as free DOX in MDA-MB-231 cells (**Figure 5**). Both free DOX, and DOX released from the NPs were easily observed in the cells, concentrated in the nuclei, which is consistent with earlier studies.[61,62] In addition, the amount of DOX in the nuclei increased after 48 h incubation compared to 4 h. This indicates that encapsulation by the NPs does not prevent DOX from being released and penetrating into the nuclei. Similar localization patterns were also found in RAW 246.7 cells, which is not a breast cancer cell line (Supporting Information Figure S15). This suggests that the efficacy of our NPs may also be applicable for other cancer types.

A localization study of the NPs was performed by incubating FITC-[G#0]-P(O-*co*-T)$_{28k}$ NPs with the two cell lines for different periods of time, and images were obtained using confocal microscopy. All cell lines were able to internalize FITC-[G#0]-P(O-*co*-T)$_{28k}$ NPs after 48 h of incubation. NPs were mainly found in the cytoplasm and concentrated at the surroundings of the nuclei with a minority overlapping with the nuclei (Supporting Information Figure S16). Unlike DOX, which is mainly concentrated in the nuclei, the NPs are considered to have very low penetration through the nuclei membrane due to their large size. The uptake rate of the NPs varied between the two cell lines, where the RAW 246.7 cells demonstrated the fastest uptake.

2.7. In Vitro ^{19}F-MRI Studies

The fluorinated NPs were further evaluated as contrast agents for ^{19}F-MRI. The measurements were conducted by loading the NPs (190-970 μM in PBS) into 6 mm diameter plastic syringes. Depending on the molecular weight of the different polymers, fluorine concentrations between 23–56 mM was achieved. The MRI phantoms (the cross-section of a syringe) seen in **Figure 6**, showing that all the materials exhibited very good imaging capability. In only 10 min scanning time (32 scans), signal-to-noise (SNR) ratios of 7–16 were achieved for all the NPs. This is most likely an effect of the high fluorine concentration of the polymers, as well as favorable chain mobility in the hydrophilic segments. However, for future practical use in vivo, the local concentration of the NPs must be sufficient to ensure high enough concentration for effective imaging. Such local concentration enhancement can be achieved via either passive (EPR effect) or active targeting measures (small molecular, peptide, or antibody based tissue specific ligand targeting).[63,64] As mentioned earlier, introduction of acrylic acid segments to the polymers will provide potential handles for such functionalization and is currently under investigation.

Recently results published by Matsuda et al.[31] reveals beneficial ^{19}F-imaging properties of statistical copolymers of 2,2,3,3-tetrafluoropropyl methacrylate and methyl acrylate (PTFPMA-*co*-PMA) grafted from PAMAM dendrimer cores due to increased fluorine mobility gained by the star-like architecture. The synthesized NPs in this study behave in a similar fashion, however; benefits from the combination of the more physiologically inert POEGMA sequences and biocompatible bis-MPA structure, in comparison to the charged and toxic PAMAM dendrimer.[65] This suggests that statistical P(OEGMA-*co*-TFEMA) copolymers may be an attractive approach to introduce diagnostic functions to drug delivery platforms.

3. Conclusions

Fluorinated NPs were successfully prepared by self-assembly of both linear and star-shaped block copolymers. Incorporation of fluorinated segments allow the NPs to be detected by ^{19}F-MRI, and the hydrophobic cores are able to encapsulate DOX, and generate thereby a versatile theranostic system. The designed core-shell type NPs are around 10 nm in size and allow for

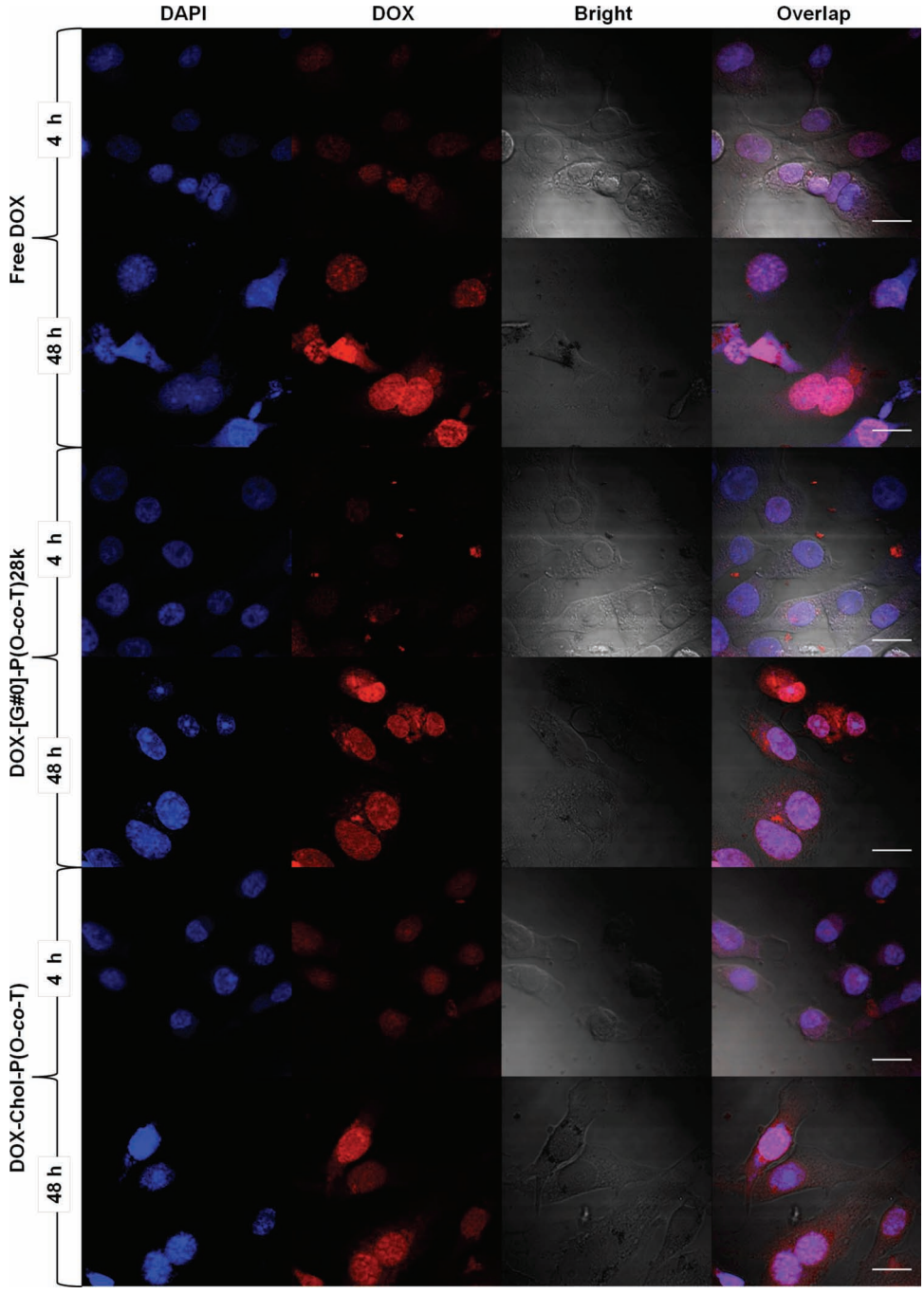

Figure 5. Localization of DOX for the MDA-MB-231 breast cancer cell line. The nuclei of the cells are stained by DAPI (blue), and DOX (red). Cells were treated with 5 μg mL^{-1} of free DOX, DOX-[G#0]-P(O-*co*-T)$_{28k}$ NPs, or DOX-Chol-P(O-*co*-T) NPs for 4 h and 48 h. Scale bar = 20 μm.

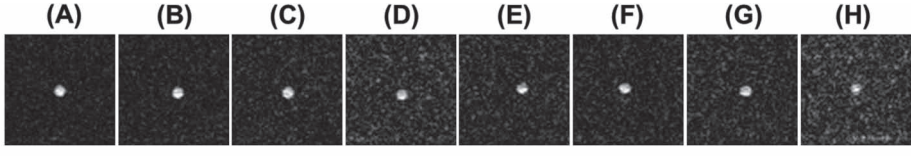

Figure 6. ^{19}F-MRI phantoms of the polymers in PBS (10 mg mL^{-1}) received after 10 min (32 scans). A) EBiB-P(O-*co*-T), B) Dod-P(O-*co*-T), C) Chol-P(O-*co*-T), D) [G#0]-P(O-*co*-T)$_{10k}$, E) [G#0]-P(O-*co*-T)$_{28k}$, F) [G#2]-P(O-*co*-T)$_{23k}$, G) [G#2]-P(O-*co*-T)$_{36k}$, and H) [G#2]-P(O-*co*-T)$_{52k}$.

high loading capacities of the drug. After loading with DOX the NPs show interparticle aggregation, however, this is proved to be significantly reduced by incorporation of negatively charged segments into the polymers. The DOX release kinetics of the nanocarriers show clear core dependence, thus suggesting that the release from the formed NPs can be tuned by the macromolecular architecture. Further, ^{19}F-NMR diffusion studies prove that the NPs are not subjected to any detectable protein adsorption in plasma, thus indicating a stealthy appearance due to the exterior POEGMA segments. Confocal studies suggest that the NPs can be taken up by breast cancer cells and deliver the drug into the cell nuclei. In addition, neat NPs proved to be non-toxic to breast cancer cells by apoptosis and MTT tests, while DOX-loaded NPs showed a dose-dependent toxicity. Conclusively, the designed fluorinated NPs show controllable drug release kinetics, are detectable by ^{19}F-MRI, and are non-toxic to breast cancer cells; they are therefore a promising approach to design a theranostic delivery system.

4. Experimental Section

Materials: Details for all reagents are provided in the Supporting Information.

Synthesis and Characterization: Details of the preparation of the polymers and instruments utilized for characterization (^{1}H- and ^{13}C-NMR, SEC, MALDI-TOF, DLS, TEM, CMC) of the fluorinated copolymers are reported in the Supporting Information, as well as the instrumentation for ^{19}F-NMR diffusion, ^{19}F-MRI, FACS, microscopy, etc.

Doxorubicin Loading: DOX stock solution was prepared by dissolving DOX and TEA (1:3 mol eq) in CH_2Cl_2 (1 mg mL^{-1}). The stock solution (1 mL) was diluted with CH_2Cl_2 (1 mL) and mixed with a phosphate buffer saline (PBS) solution of NPs (4 mL, 1.25 mg mL^{-1}). The mixture was stirred overnight at 100 rpm in order to evaporate the organic solvent. Free DOX was removed by spin filtration with a MWCO of 3 kDa by refilling PBS every 5 min. The concentration of DOX in NPs was measured by comparing UV absorbance at 490 nm, of samples diluted with DMF:H_2O (4:1) to a standard curve (five replicates).

In Vitro Drug Release: DOX or DOX-NPs solutions were transferred into dialysis cassettes (MWCO 3500, Slide-A-Lyzer, Thermo) containing 3 mL PBS for each sample. Cassettes were suspended in 4 L of PBS. Aliquots from the cassettes were collected (triplicates of 10 µL each) at the following time intervals: 0, 2, 4, 8, 12, 24, 48, and 72 h. Thereafter, the samples were transferred into fluorescence plates, containing 100 µL DMF:H_2O (4:1) and diluted with 100 µL PBS. The fluorescence intensity of samples was determined using a plate reader (BioTek Synergy MX) at wavelength 480/600 (excitation/emission) nm.[66]

^{19}F-NMR and ^{19}F-NMR Diffusion: ^{19}F-NMR was employed to determine longitudinal (T_1) and transverse (T_2) relaxation times, and self-diffusion of the molecules for size determination in different media. For all ^{19}F NMR studies, the different samples were dissolved at 0.5% (w/w) in the given solvents. The measurements were performed at 37 (± 0.1) °C on a Bruker 600 MHz Avance spectrometer operating at 564 MHz for ^{19}F, equipped with a Diff30 diffusion probe. To collect T_1 data an inversion recovery pulse sequence was used and for T_2 a CPMG pulse sequence was accumulated. Self-diffusion measurements were performed using NMR diffusometry (NMRd).[67,68] Additional information about the NMR diffusion studies can be found in the Supporting Information as well as detailed instrumentation details and supplemental physiochemical and in vitro results.

Cellular-Based Tests: Human breast cell lines MDA-MB-231, MDA-MB-468 cells and MCF-7 and mouse monocyte macrophage cell line RAW 264.7 were cultured in DMEM (pH 7.4) containing 10% (v/v) FBS, 100 U mL^{-1} penicillin, and 2 mM glutamine solution at 37 °C in a humidified atmosphere with 5% CO_2. The three breast cancer cells were harvested by trypsin while RAW 264.7 was harvested by scraping. MTT assay was preceded for cellular viability tests. The four different cells were separately seeded into 96-well plates, and the concentration was adjusted to 5×10^4 cells per well (in 100 µL DMEM) and finally cultured for 24 h. The medium was removed and the plate was refilled with 100 µL of fresh medium containing various concentrations of the NPs, DOX-NPs, and DOX (4 parallel wells for each concentration). The cells were incubated for another 48 h or 72 h before 10 µL MTT solution (5 mg mL^{-1}) was added to each well. Thereafter, the cells were incubated for additional 4 h, and 100 µL SDS solutions (10%) were added to each well. The absorbance was measured after 18 h in a plate reader at 570 nm.[6] The details of other cell based experiments, including apoptosis/necrosis, uptake and localization studies are reported in the Supporting Information.

Statistical Analysis: Dynamic light scattering, cell viability tests, drug release and uptake studies are presented as mean values with standard deviation (SD). For the uptake studies statistical analysis was performed with the Student's t-test and $p < 0.001$ was considered significant. The drug release curve and IC_{50} curves were plotted in KaleidaGraph v4.1 (Synergy Software, Reading, PA).

Supporting Information

Supporting Information is available from the Wiley Online Library or from the author.

Acknowledgements

C.P. and Y.Z. contributed equally to this work. Funding support by the Royal Swedish Academy of Sciences, Falk Foundation, Jeanssons Foundation, Axel and Eva Wallströms Foundation, Södra AB, and the Swedish Research Council (VR), under grants 2011-3720 and 2009-3259, are gratefully acknowledged. A.M.N. is the recipient of an assistant professorship from Carl Bennet AB, Karolinska Institutet and Vinnova.

Received: January 15, 2013

[1] M. J. Piccart-Gebhart, M. Procter, B. Leyland-Jones, A. Goldhirsch, M. Untch, I. Smith, L. Gianni, J. Baselga, R. Bell, C. Jackisch, D. Cameron, *N. Engl. J. Med.* **2005**, *353*, 1659.
[2] S. C. Piscitelli, K. A. Rodvold, D. A. Rushing, D. A. Tewksbury, *Clin. Pharmacol. Ther.* **1993**, *53*, 555.
[3] D. Raghavan, W. U. Shipley, M. B. Garnick, P. J. Russell, J. P. Richie, *N. Engl. J. Med.* **1990**, *322*, 1129.
[4] T. A. Yap, C. P. Carden, S. B. Kaye, *Nat. Rev. Cancer* **2009**, *9*, 167.
[5] J. H. Doroshow, *N. Engl. J. Med.* **1991**, *324*, 843.
[6] X. H. Zeng, Y. N. Zhang, Z. H. Wu, P. Lundberg, M. Malkoch, A. M. Nyström, *J. Polym. Sci. Part A Polym. Chem.* **2012**, *50*, 280.
[7] V. P. Torchilin, *Nat. Rev. Drug Discovery* **2005**, *4*, 145.
[8] D. Peer, J. M. Karp, S. Hong, O. C. Farokhzad, R. Margalit, R. Langer, *Nat. Nanotechnol.* **2007**, *2*, 751.
[9] R. Duncan, *Nat. Rev. Cancer* **2006**, *6*, 688.
[10] Y.-X. Zhao, A. Shaw, X. Zeng, E. Benson, A. M. Nyström, B. Högberg, *ACS Nano* **2012**, *6*, 8684.
[11] D. Kim, E. S. Lee, K. T. Oh, Z. G. Gao, Y. H. Bae, *Small* **2008**, *4*, 2043.
[12] S. H. Medina, M. E. H. El-Sayed, *Chem. Rev.* **2009**, *109*, 3141.
[13] J. You, G. D. Zhang, C. Li, *ACS Nano* **2010**, *4*, 1033.
[14] M. Ferrari, *Nat. Rev. Cancer* **2005**, *5*, 161.
[15] V. P. Torchilin, *Pharm. Res.* **2007**, *24*, 1.

[16] K. Kataoka, G. S. Kwon, M. Yokoyama, T. Okano, Y. Sakurai, *J. Controlled Release* **1993**, *24*, 119.
[17] T. M. Allen, P. R. Cullis, *Science* **2004**, *303*, 1818.
[18] A. M. Nyström, K. L. Wooley, *Acc. Chem. Res.* **2011**, *44*, 969.
[19] J. R. McCarthy, F. A. Jaffer, R. Weissleder, *Small* **2006**, *2*, 983.
[20] S. S. Kelkar, T. M. Reineke, *Bioconjugate Chem.* **2011**, *22*, 1879.
[21] S. M. Janib, A. S. Moses, J. A. MacKay, *Adv. Drug Delivery Rev.* **2010**, *62*, 1052.
[22] Y. Liu, N. Zhang, *Biomaterials* **2012**, *33*, 5363.
[23] T. L. Kalber, N. Kamaly, S. A. Higham, J. A. Pugh, J. Bunch, C. W. McLeod, A. D. Miller, J. D. Bell, *Bioconjugate Chem.* **2011**, *22*, 879.
[24] C. Sanson, O. Diou, J. Thevenot, E. Ibarboure, A. Soum, A. Brulet, S. Miraux, E. Thiaudiere, S. Tan, A. Brisson, V. Dupuis, O. Sandre, S. Lecommandoux, *ACS Nano* **2011**, *5*, 1122.
[25] N. Nasongkla, E. Bey, J. M. Ren, H. Ai, C. Khemtong, J. S. Guthi, S. F. Chin, A. D. Sherry, D. A. Boothman, J. M. Gao, *Nano Lett.* **2006**, *6*, 2427.
[26] X. Q. Yang, J. J. Grailer, I. J. Rowland, A. Javadi, S. A. Hurley, V. Z. Matson, D. A. Steeber, S. Q. Gong, *ACS Nano* **2010**, *4*, 6805.
[27] G. Liu, J. Gao, H. Ai, X. Chen, *Small* **2012**, DOI: 10.1002 / smll.201201531.
[28] A. M. Nyström, J. W. Bartels, W. Du, K. L. Wooley, *J. Polym. Sci. Part A Polym. Chem.* **2009**, *47*, 1023.
[29] W. Du, Z. Xu, A. M. Nyström, K. Zhang, J. R. Leonard, K. L. Wooley, *Bioconjugate Chem.* **2008**, *19*, 2492.
[30] W. J. Du, A. M. Nyström, L. Zhang, K. T. Powell, Y. L. Li, C. Cheng, S. A. Wickline, K. L. Wooley, *Biomacromolecules* **2008**, *9*, 2826.
[31] M. Ogawa, H. Kataoka, S. Nitahara, H. Fujimoto, H. Aoki, S. Ito, M. Narazaki, T. Matsuda, *Bull. Chem. Soc. Jpn.* **2012**, *85*, 79.
[32] H. Peng, I. Blakey, B. Dargaville, F. Rasoul, S. Rose, A. K. Whittaker, *Biomacromolecules* **2009**, *10*, 374.
[33] K. J. Thurecht, I. Blakey, H. Peng, O. Squires, S. Hsu, C. Alexander, A. K. Whittaker, *J. Am. Chem. Soc.* **2010**, *132*, 5336.
[34] M. Ogawa, S. Nitahara, H. Aoki, S. Ito, M. Narazaki, T. Matsuda, *Macromol. Chem. Phys.* **2010**, *211*, 1369.
[35] A. Kieger, M. J. Wiester, D. Procissi, T. B. Parrish, C. A. Mirkin, C. S. Thaxton, *Small* **2011**, *7*, 1977.
[36] J.-F. Lutz, *J. Polym. Sci. Part A Polym. Chem.* **2008**, *46*, 3459.
[37] D. A. C. Thomson, E. H. L. Tee, N. T. D. Tran, M. J. Monteiro, M. A. Cooper, *Biomacromolecules* **2012**, *13*, 1981.
[38] R. F. T. Stepto, *Polym. Int.* **2010**, *59*, 23.
[39] M. M. Kaneda, S. Caruthers, G. M. Lanza, S. A. Wickline, *Ann. Biomed. Eng.* **2009**, *37*, 1922.
[40] M. Srinivas, A. Heerschap, E. T. Ahrens, C. G. Figdor, I. J. M. de Vries, *Trends Biotechnol.* **2010**, *28*, 363.
[41] W. Du, Y. Li, A. M. Nyström, C. Cheng, K. L. Wooley, *J. Polym. Sci. Part A Polym. Chem.* **2010**, *48*, 3487.
[42] H. S. Choi, W. Liu, P. Misra, E. Tanaka, J. P. Zimmer, B. I. Ipe, M. G. Bawendi, J. V. Frangioni, *Nat. Biotechnol.* **2007**, *25*, 1165.
[43] M. E. Fox, F. C. Szoka, J. M. J. Frechet, *Acc. Chem. Res.* **2009**, *42*, 1141.
[44] T. Etrych, V. Subr, J. Strohalm, M. Sirova, B. Rihova, K. Ulbrich, *J. Controlled Release* **2012**, *164*, 346.
[45] K. Kalyanasundaram, J. K. Thomas, *J. Am. Chem. Soc.* **1977**, *99*, 2039.
[46] M. A. Dobrovolskaia, A. K. Patri, J. Zheng, J. D. Clogston, N. Ayub, P. Aggarwal, B. W. Neun, J. B. Hall, S. E. McNeil, *Nanomedicine* **2009**, *5*, 106.
[47] A. M. Nyström, Z. Xu, J. Xu, S. Taylor, T. Nittis, S. A. Stewart, J. R. Leonard, K. L. Wooley, *Chem. Commun.* **2008**, 3579.
[48] S. Abraham, F. Guo, L. S. Li, C. Rader, C. Liu, C. F. Barbas, R. A. Lerner, S. C. Sinha, *Proc. Natl. Acad. Sci. USA* **2007**, *104*, 5584.
[49] M. B. Gariboldi, R. Ravizza, R. Molteni, D. Osella, E. Gabano, E. Monti, *Cancer Lett.* **2007**, *258*, 181.
[50] Z. Wang, W. K. Chui, P. C. Ho, *Pharm. Res.* **2009**, *26*, 1162.
[51] C. Mamot, D. C. Drummond, U. Greiser, K. Hong, D. B. Kirpotin, J. D. Marks, J. W. Park, *Cancer Res.* **2003**, *63*, 3154.
[52] M. A. Tapia, I. Gonzalez-Navarrete, A. Dalmases, M. Bosch, V. Rodriguez-Fanjul, M. Rolfe, J. S. Ross, J. Mezquita, C. Mezquita, O. Bachs, P. Gascon, F. Rojo, R. Perona, A. Rovira, J. Albanell, *Cell Cycle* **2007**, *6*, 2284.
[53] D. Ren, F. Kratz, S. W. Wang, *Small* **2011**, *7*, 1051.
[54] F. T. Andon, B. Fadeel, *Acc. Chem. Res.* **2012**.
[55] F. A. Fornari, J. K. Randolph, J. C. Yalowich, M. K. Ritke, D. A. Gewirtz, *Mol. Pharmacol.* **1994**, *45*, 649.
[56] S. H. Kaufmann, W. C. Earnshaw, *Exp. Cell Res.* **2000**, *256*, 42.
[57] S. Fulda, K. M. Debatin, *Oncogene* **2006**, *25*, 4798.
[58] B. Kalyanaraman, J. Joseph, S. Kalivendi, S. W. Wang, E. Konorev, S. Kotamraju, *Mol. Cell. Biochem.* **2002**, *234*, 119.
[59] F. Danhier, N. Lecouturier, B. Vroman, C. Jerome, J. Marchand-Brynaert, O. Feron, V. Preat, *J. Controlled Release* **2009**, *133*, 11.
[60] K. Kim, M. Lee, H. Park, J. H. Kim, S. Kim, H. Chung, K. Choi, I. S. Kim, B. L. Seong, I. C. Kwon, *J. Am. Chem. Soc.* **2006**, *128*, 3490.
[61] J. A. MacKay, M. N. Chen, J. R. McDaniel, W. G. Liu, A. J. Simnick, A. Chilkoti, *Nat. Mater.* **2009**, *8*, 993.
[62] A. A. Bhirde, A. Kapoor, G. Liu, R. Iglesias-Bartolome, A. Jin, G. F. Zhang, R. J. Xing, S. Lee, R. D. Leapman, J. S. Gutkind, X. Y. Chen, *ACS Nano* **2012**, *6*, 4966.
[63] H. Maeda, *Bioconjugate Chem.* **2010**, *21*, 797.
[64] Y. Matsumura, H. Maeda, *Cancer Res.* **1986**, *46*, 6387.
[65] N. Feliu, M. V. Walter, M. I. Montanez, A. Kunzmann, A. Hult, A. Nyström, M. Malkoch, B. Fadeel, *Biomaterials* **2012**, *33*, 1970.
[66] Z. H. Wu, X. H. Zeng, Y. N. Zhang, N. Feliu, P. Lundberg, B. Fadeel, M. Malkoch, A. M. Nystrom, *J. Polym. Sci. Part A Polym. Chem.* **2012**, *50*, 217.
[67] P. Stilbs, *Prog. Nucl. Magn. Reson. Spectrosc.* **1987**, *19*, 1.
[68] W. S. Price, *Concepts Magn. Reson.* **1997**, *9*, 299.